MERCK

catch the sun

Product Category list:

- Organic Photovoltaic (OPV) Donors and Acceptors
- Dye-Sensitized Solar Cell Materials
- Perovskite Materials

Visit us at:
SigmaAldrich.com/organic-electronics

MK_AD9792EN 43729 08/2022

The Life Science business of Merck operates as MilliporeSigma in the U.S. and Canada.

Sigma-Aldrich®
Lab & Production Materials

FULL PAPER

Evolution of Hot Polaron States with a Nanosecond Lifetime in a Manganite Perovskite

*Dirk Raiser, Stephanie Mildner, Benedikt Ifland, Mohsen Sotoudeh, Peter Blöchl, Simone Techert, and Christian Jooss**

Understanding and controlling the relaxation process of optically excited charge carriers in solids with strong correlations is of great interest in the quest for new strategies to exploit solar energy. Usually, optically excited electrons in a solid thermalize rapidly on a femtosecond to picosecond timescale due to interactions with other electrons and phonons. New mechanisms to slow down thermalization will thus be of great significance for efficient light energy conversion, e.g., in photovoltaic devices. Ultrafast optical pump–probe experiments in the manganite $Pr_{0.65}Ca_{0.35}MnO_3$, a photovoltaic, thermoelectric, and electrocatalytic material with strong polaronic correlations, reveal an ultraslow recombination dynamics on a nanosecond-time scale. The nature of long living excitations is further elucidated by photovoltaic measurements, showing the presence of photodiffusion of excited electron–hole polaron pairs. Theoretical considerations suggest that the excited charge carriers are trapped in a hot polaron state. Escape from this state is possible via a slow dipole-forbidden recombination process or via rare thermal fluctuations toward a conical intersection followed by a radiation-less decay. The strong correlation between the excited polaron and the octahedral dynamics of its environment appears to be substantial for stabilizing the hot polaron.

1. Introduction

Searching new mechanisms with enhanced lifetimes of hot charge carrier excitations is of huge importance for improving the efficiency of photovoltaic and photochemical energy conversion.[1] Generally, the lifetime of hot charge carriers is determined by the collisions with electrons, phonons or spins as well as the requirement of energy-momentum conservation during electron–hole recombination. In the case of metals, where the excitation energy is not restricted by a bandgap, hot carriers directly relax into thermal equilibrium. The lifetime of electronic excitations is thus limited to a few femtoseconds. In semiconductors, the lifetime of interband excitations can be dramatically increased, by the large energy and momentum separation of photoexcited electron and hole states[2,3] and can even reach hundreds of milliseconds in clean indirect bandgap systems.

The mechanism of electron–hole recombination can be entirely modified by strong electronic and electron–lattice correlations. For example, optical excitations in Mott-insulators are expected to show enhanced lifetimes due to the suppression of spin-relaxation channels.[4] Theoretical work suggests that excitations of small polarons, i.e., quasiparticles which are formed by strong electron–phonon interactions, can exhibit large lifetimes due to the formation of delocalized metastable states.[5] Experiments in molecular systems reveal that large lifetimes of polaronic excitations require, that electron–hole recombination by dipole-allowed radiative processes as well as by fast structural relaxation through a conical intersection between the potential-energy surfaces of different electronic states must be avoided.[6] The latter requires, that the minimum on an excited energy surface is well separated from a conical intersection.

In this work, we study the temporal evolution of a hot polaron state with a long lifetime in a hole-doped manganite $Pr_{1-x}Ca_xMnO_3$ (PCMO) with high carrier concentration of $\approx 3 \times 10^{21}$ cm^{-3} at $x = 0.35$. Moreover, we substantiate the existence of long-living hot polarons by measurements of the open-circuit voltage of a $Pr_{1-x}Ca_xMnO_3$-based photovoltaic device at the same doping level. In the doping range $0.3 < x < 0.5$, charge carriers in $Pr_{1-x}Ca_xMnO_3$ form an interacting dense system of small polarons.[7–9] Below the charge-ordering (CO) transition

D. Raiser, Prof. S. Techert
Structural Dynamics of (Bio)chemical Systems
Max-Planck-Institute for Biophysical Chemistry
Am Faßberg 11, D-37077 Goettingen, Germany
Dr. S. Mildner, B. Ifland, Prof. P. Blöchl, Prof. Ch. Jooss
Institute for Material Physics
University of Goettingen
Friedrich-Hund-Platz 1, D-37077 Goettingen, Germany
E-mail: jooss@material.physik.uni-goettingen.de
M. Sotoudeh, Prof. P. Blöchl
Institute for Theoretical Physics
University of Clausthal
Leibnizstrasse 10, D-38678 Clausthal-Zellerfeld, Germany
D. Raiser, Prof. S. Techert
FS Structural Dynamics in Chemical Systems
Deutsches Elektronensynchrotron DESY
Notkestrasse 85, D-22607 Hamburg, Germany
Prof. S. Techert
Institute for X-ray Physics
University of Goettingen
Friedrich-Hund-Platz 1, D-37077 Goettingen, Germany

DOI: 10.1002/aenm.201602174

temperature $T_{CO} \approx 240$ K, the polaron liquid crystallizes and forms a charge-ordered state (see Figure S5, Supporting Information). Several manganites such as $Pr_{1-x}Ca_xMnO_3$, $La_{1-x}Ca_xMnO_3$ (LCMO) and the semiconducting phase of $La_{1-x}Sr_xMnO_3$ (LSMO) exhibit a strong small polaron IR optical absorption feature between 500 meV and 2 eV,[10–13] followed by charge-transfer (CT) transitions at higher energies. **Figure 1**a shows the optical conductivity. The broad maximum in optical conductivity at around 1.5 eV is typical for narrow-bandwidth manganites and is a fingerprint for small-polaron absorption.[11,14,15]

This absorption band at about 1.5 eV is generally attributed to a transition between Jahn–Teller (JT) split Mn 3d e_g states (Figure 1b), either occurring as an intrasite or as an intersite transition between Mn^{3+} and Mn^{4+} sites.[12,16,17] The transition

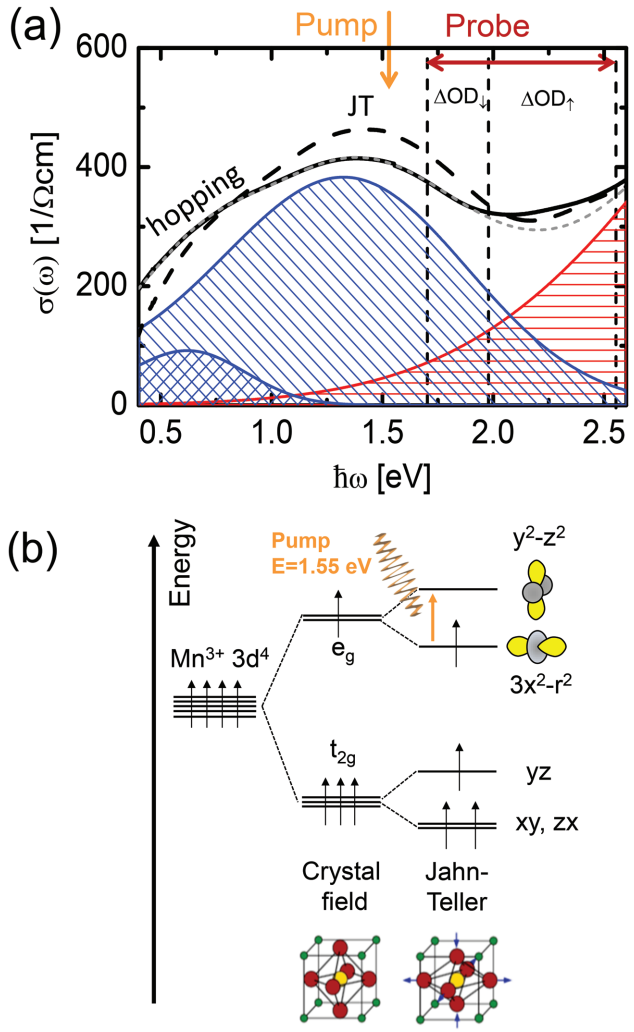

Figure 1. Optical absorption experiments at energies close to the JT splitting of Mn 3d e_g–O 2p states of an epitaxial $Pr_{0.65}Ca_{0.35}MnO_3$ film. a) Measured optical conductivity with indicated energies of the pump and the probe pulses. The results are obtained from transmission spectroscopy at 300 K (bold line) and 80 K (broken line). The gray line is the result of peak fitting at 300 K. The main peak at the JT energy is broadened towards lower energies due to the presence of polaron hopping. The red tail results from CT transitions at higher energy. b) Scheme of the crystal field splitting and the JT splitting of the degenerated Mn 3d levels in undoped $PrMnO_3$.

is broadened by a polaron hopping feature at 0.5–0.8 eV and coupling to a phonon bath. The JT effect describes the formation of polarons via strong electron–phonon coupling between an electron in a pair of degenerate electron states and nuclear distortions, i.e., phonons that lift the degeneracy by lowering the underlying symmetry.[18] In manganites, the involved electronic states are the two Mn 3d e_g states pointing toward the oxygen neighbors and the JT active nuclear distortions encompass combinations of prolate and oblate distortions of the MnO_6 octahedra along the three axes. The energy gain of involved Mn 3d e_g states is comprised by an electronic energy gain $-2E_0$ and the energy $+E_0$ expended for lattice deformation.[19] E_0 typically is of the order of 0.2–0.6 eV in manganites for $x \leq 0.5$.[12,20]

In a single JT active MnO_6 octahedron, an optical transition from the lower to the upper Mn 3d e_g states at $\Delta E = 4\ E_0$ is dipole forbidden and can therefore not explain the observed dominant spectral absorption band in manganites. Similarly, radiative decay of the excited JT polaron is suppressed by the optical selection rules. However, such an excited state would rapidly depopulate by a radiation-less transition through a conical intersection.[21] This transition involves nuclear distortions and would occur within a few periods of a JT active vibrational mode, that is, on a sub-picosecond timescale.[22] Such a rapid decay of a JT excitation is, however, in contrast with our findings for $Pr_{0.65}Ca_{0.35}MnO_3$ reported below. It furthermore seems to contradict the observed long lifetimes of polaron excitations of up to 1 ns in the semiconducting phase of $La_{0.7}Ca_{0.3}MnO_3$[23,24] and several nanoseconds in $Nd_{0.5}Sr_{0.5}MnO_3$,[25] all measured at pump energies of $E = 1.55$ eV $\approx 4\ E_0$. The origin of the long lifetimes is controversially discussed. Whereas Ren et al.[26] attribute the long lifetime in LCMO to a localized metastable state, the ns decay of optical density is simply interpreted as heat diffusion from the film into the substrate by Bielecki et al.[27] In $Nd_{0.5}Sr_{0.5}MnO_3$, the long polaron lifetime is even considered as a prerequisite for the observed optically induced phase transitions at high photon intensities.[25]

2. Results

2.1. Photovoltaic Measurements

In order to evaluate the presence of photodiffusion of electron–hole pairs excited at a photon energy of 1.55 eV in the PCMO, the photovoltaic effect in a junction formed with an electron-doped $SrTi_{1-y}Nb_yO_3$ ($y = 0.002$) (STNO) substrate is measured. The open-circuit voltage V_{OC} as a function of temperature measured under monochromatic illumination at 1.55 eV is shown in **Figure 2**a. Below the charge-ordering temperature at $T_{CO} \approx 200$ K, V_{OC} shows a linear increase toward lower temperatures with an intercept at $V_{OC}(T = 0) = 520$ meV, which represents the barrier for polaronic charge separation at the interface (see also Section 15, Supporting Information). A linear temperature dependence of V_{OC} reflects that charge separation is determined by the barrier for the recombination current.[28,29] Thus excess carrier accumulation at the junction is not limited by photodiffusion of excited minority carriers, i.e., their diffusion length is larger than the space charge region of the junction.

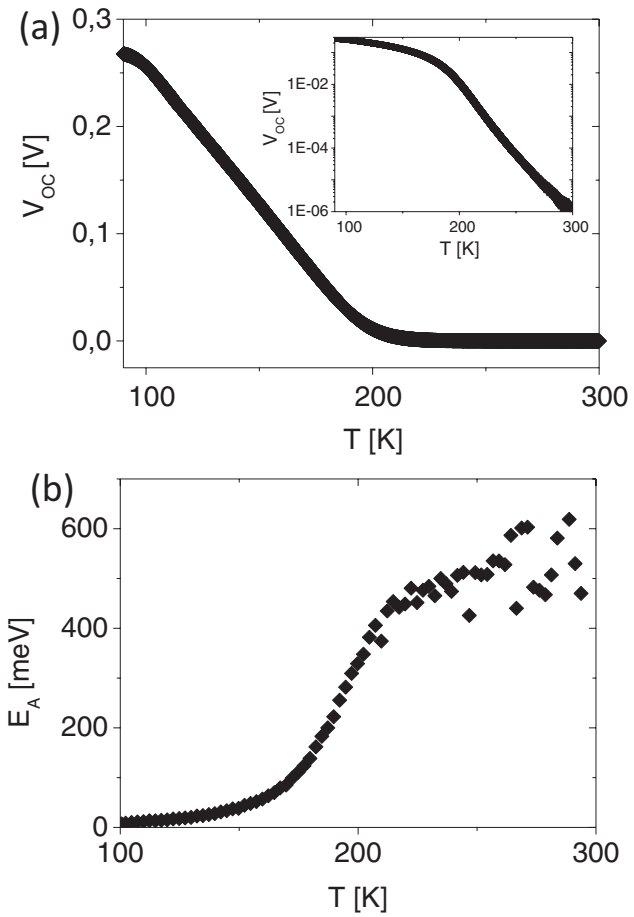

Figure 2. Photovoltaic effect in a PCMO/Nb:STO heterojunction under monochromatic illumination at $E = 1.55$ eV. a) Photovoltage under open-circuit conditions V_{OC} as a function of temperature. The linear behavior below T_{CO} is due to bulk photodiffusion of electron–hole pairs. Above T_{CO}, there is a cross over into thermally activated exponential temperature dependence (logarithmic representation in the inset). b) Temperature dependence of the apparent activation energy E_A determined from V_{OC} (T) in (a). The strong drop below TCO is due to cross over from activated interface to bulk photodiffusion of carriers.

By contrast, above T_{CO}, an exponential temperature dependence of V_{OC} is observed (Figure 2a, inset). It is reflecting a limitation of the photovoltage by interface excitations. The apparent activation energy E_A is determined from the logarithmic derivative (Figure 2b). It shows a plateau value of $E_A = 515 \pm 30$ meV between 220 and 300 K (equalling the barrier for the recombination current) and has a strong drop of E_A below 220 K due to the onset of the bulk diffusion of photocarriers in the manganite. Because of the bandgap of 3.3 eV in STNO, photon absorption at the pump energy is absent at the n-doped material and the photovoltage is entirely generated by photogeneration of charge carriers in the hole-doped PCMO film.

2.2. Transient Absorbance Measurements

The time evolution of the polaron excitation at $E = 1.55$ eV is studied by optical pump–probe spectroscopy, revealing the induced change in the optical density ΔOD of an epitaxial PCMO ($x = 0.35$) thin film grown on MgO in transmission configuration. Details concerning the measurement, its parameters and the properties of the film are provided in the Supporting Information (see Sections 1 and 2).

Figure 3 gives an overview on the temporal and spectral change of the optical density at energies slightly above the excitation energy. We observe a drop of ΔOD due to ground-state bleaching. This effect can be probed up to a photon energy of 2.2 eV. In addition, there is an increase of the OD at energies above 2.4 eV at temperatures $T > 150$ K.

From the temporal evolution of the obtained spectra, four processes can be distinguished:

- Process (i): An ultrafast change of ΔOD on a time scale of <200 fs caused by the absorption of the pump pulse, which can be either negative (below 2.2 eV) or positive (above 2.4 eV). The temporal evolution of this process cannot be resolved with our setup.
- Process (ii): A fast relaxation of the ΔOD from a maximum value on a short time scale ($\tau_{fast} \approx 980$ fs), which is independent of whether the total ΔOD is positive or negative. This process is superimposed by coherent oscillations in the THz range, which we in the following discuss as process (iii). The exponential decrease of the signal is characterized by its amplitude A_{fast}, its decay time τ_{fast}, and its stretching factor b_{fast}.
- Process (iii): Coherent oscillations of the ΔOD with a dominant frequency of 25 GHz ($t_{coh} \approx 40$ ps) and several additional frequency bands, which extend up to the THz range.
- Process (iv): A slow relaxation of ΔOD on a long time scale of $\tau_{slow} \approx 1$–2 ns. This relaxation process is superimposed by the low frequency GHz oscillations described in process (iii). Its exponential decrease is characterized by its amplitude A_{slow}, its decay time τ_{slow} and its stretching factor b_{slow}.

Since in the energy range from 2.4 to 2.6 eV, where a positive change of ΔOD is observed, charge-transfer (CT) transitions are involved, we focus in the following on the temporal evolution of the ΔOD in the energy range of $E = 1.77$–2.07 eV, where the small polaron transition is dominant. To account for the cooperative response of the polarons in PCMO we use a stretched exponential fit function with variable exponent b according to the Johnson–Mehl–Avrami–Kolmogorow (JMAK) model, which turned out to be an expedient model to recognize and characterize optical induced phase transitions in manganites.[30] However, the fit exponent b is only marginally addressed here. An extensive analysis of b in the framework of the JMAK model will be subject of a forthcoming paper. Details of the fitting procedures for the analysis the processes (ii)–(iv) are provided in Sections 6–11 of the Supporting Information.

2.3. Fast Relaxation Process (ii)

Figure 4 shows the spectral and temperature dependence of the fast relaxation process (ii). We find that both the absolute

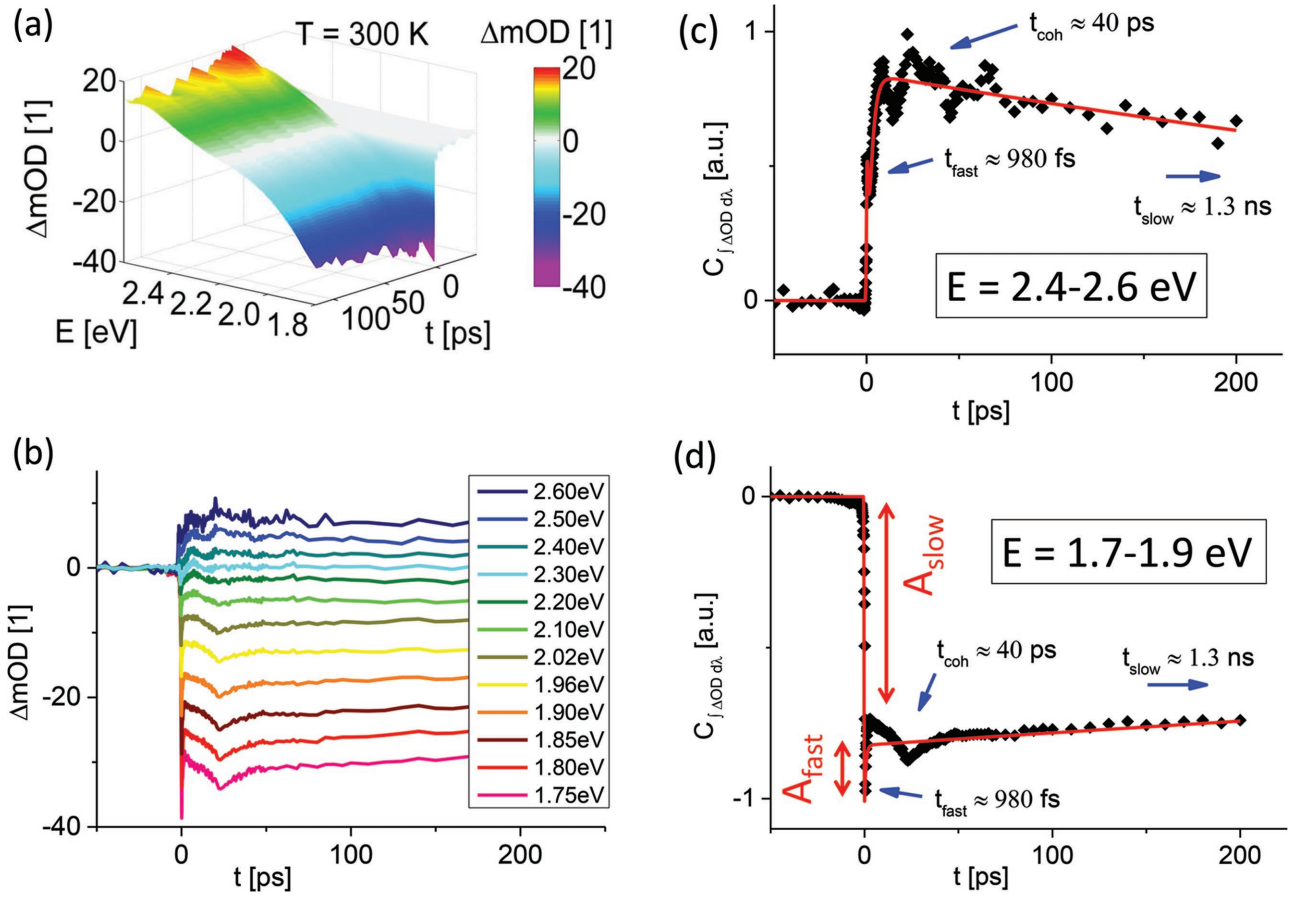

Figure 3. Time-resolved transient changes of the optical density ΔOD of an epitaxial $Pr_{0.65}Ca_{0.35}MnO_3$ thin film after ultrafast photoexcitation at $E = 1.55$ eV at room temperature. a) Photon energy and time-dependent 3D plot of ΔmOD (ΔOD/10^3). b) Line-wise cut through at different energies. c,d) Correlation functions of the integral intensities of two selected energy ranges. In both cases a multiexponential fit is applied and implemented as a red line (see Section 6, Supporting Information).

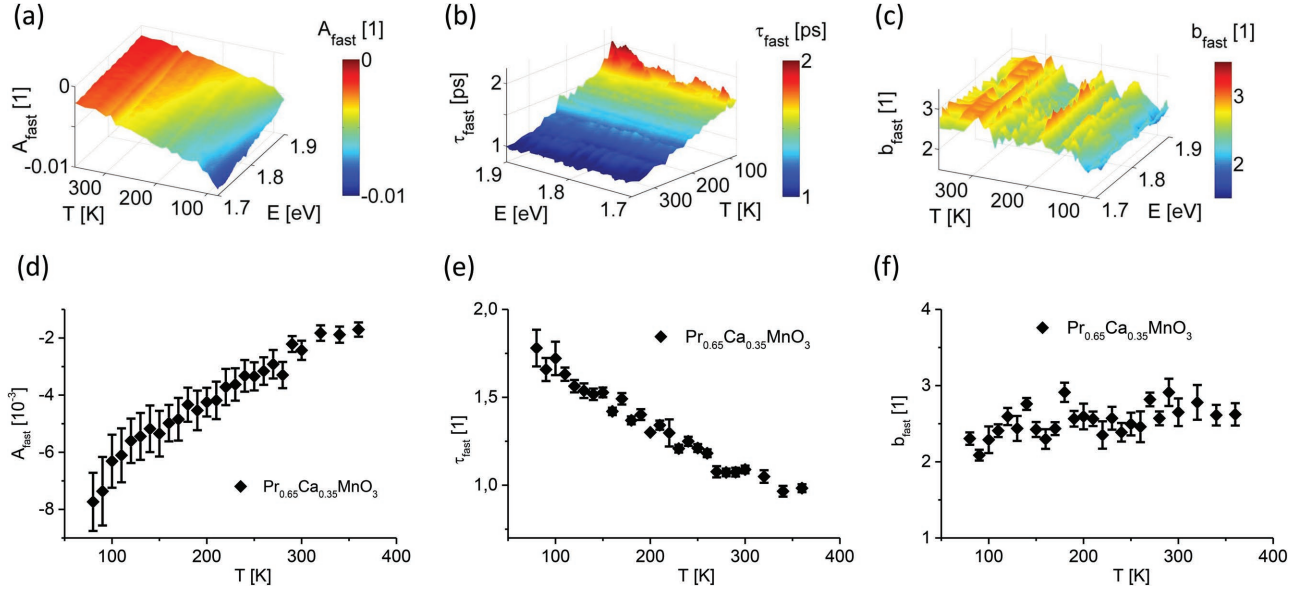

Figure 4. Energy and temperature dependency of the fast relaxation process (ii) in the ΔOD. a) The amplitude, b) the decay time, and c) the stretching factor of this process are shown as a function of temperature and probe energy. Mean values along the probe energy for d) the amplitude, e) the decay time, and f) the stretching factor.

value of the amplitude A_{fast} as well as the relaxation time τ_{fast} decreases monotonously with rising temperature. The spectrally averaged values of the relaxation time are 1.78 ps for low temperatures and 980 fs for high temperatures. Furthermore, the absolute value of the amplitude A_{fast} increases with decreasing probe energy and is largest close to the fundamental energy of the pump pulse. The resulting stretching factor b_{fast} is relatively constant and lies between 2 and 3. In order to analyze the temperature dependence of the fast relaxation process, the values of all three parameters averaged over the energy range of $E = 1.7$–1.9 eV are shown in Figure 4 d–f. The strong increase of τ_{fast} with decreasing temperature points to a thermally activated fast relaxation channel due to the interaction of the excited polaron with a thermally populated species. No fingerprint of the charge-order phase transition at $T \approx 240$ K is visible.

2.4. Coherent Oscillations (iii)

Figure 5 shows the analysis of the frequency spectrum of coherent phonon oscillations, which are superimposed to the fast relaxation process and which have a damping coefficient of about 3.4 ps (see Section 9, Supporting Information). Due to the given temporal resolution limit, frequency bands at higher phonon frequencies than those shown cannot be ruled out. A dominant frequency band at $f \approx 2.2$ THz ($E = 9$ meV) is observed for all temperatures and becomes even more pronounced at low temperatures. This frequency band is also observed in ultrafast X-ray crystallography of the JT distortion.[31] This mode is only visible, while probing the ΔOD at low energies close to the JT peak maximum. Figure 5d shows the normalized temperature evolution of the amplitude of this phonon mode. This phonon mode is rather absent above the charge-ordering temperature, which indicates its origin in the collective octahedral dynamics in the CO state.

Further coherent phonon modes exist in a spectral range between 0.5 and 4 THz. There are three main modes at around 1 THz (4.2 meV), at 2.2 THz (9 meV) and 3.9 THz (16 meV). Since they all evolve only below T_{CO}, they clearly correspond to the CO state. Although the 1 THz and 2.2 THz processes scatter strongly, they can be fitted by a phase step function, which bends up at around the CO phase transition temperature (Figure 5c,d). This is to some extent also the case for the 3.5–4 THz bands, however, the correlation function is more scattered and thus not shown. In addition to the coherent lattice oscillation in the THz regime, there is a pronounced

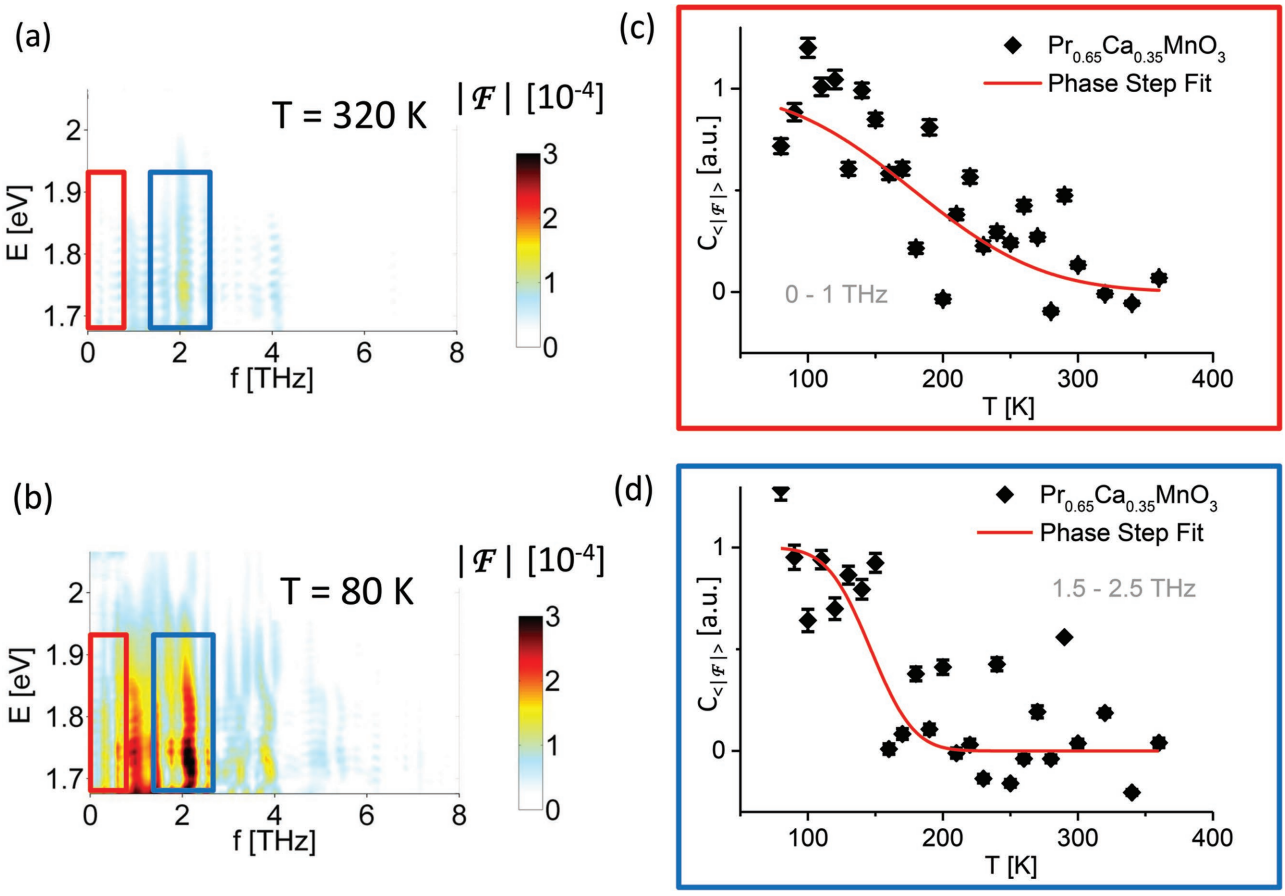

Figure 5. a,b) 2D color-coded wavelength dependency of the absolute values of the Fourier transform | F | of the OD oscillations of $Pr_{0.65}Ca_{0.35}MnO_3$ shown exemplary at two different temperatures. c,d) Correlation functions of the mean values of certain sections of the graphs shown on the left for different frequency bands. The corresponding sections are indicated by colored boxes. The central temperature of the phase transition was fitted to $T = 178(14)$ K with a width of 76(19) K for frequencies below 1 THz and to $T = 147(9)$ K with a width of 25(12) K for frequencies around 2 THz. For other frequency bands a phase transition fit was not applicable.

coherent oscillation with a period of about 40 ps (≈25 GHz) (see Figure 3). The in-depth analysis for the whole frequency range up to 4 THz can be found in the Supporting Information (Section 9).

2.5. Slow Relaxation Process (iv)

Figure 6 shows the spectral and temperature dependence of the slow relaxation process (iv). We find that the absolute value of the amplitude A_{slow} monotonously increases with decreasing temperature (Figure 6a). A_{slow} also increases with decreasing probe energy toward the fundamental of the photoexcitation

$$C_{A_{slow}}(T) = \left\langle c_{A_{slow}}(T, E) \right\rangle_E$$
$$\text{with } c_{A_{slow}}(T,E) = -\frac{A_{slow}(T, E) - A_{slow}(360\text{ K}, E)}{A_{slow}(80\text{ K}, E) - A_{slow}(360\text{ K}, E)} \quad (1)$$

The negative sign in the temperature-dependent correlation function $c_{A_{slow}}$ is due to the decrease of the absolute values of A_{slow} with increasing temperature. The temperature-dependent correlation function $C_{A_{slow}}$ is best described by a nonlinear phase step fit and thus reflects the phase transition to the charge-ordered phase at around $T \approx 240$ K, which is broadened due to an extended two phase region of charge-ordered and charge-disordered nanoscale domains.[32] Remarkably, the relaxation time τ_{slow} monotonously increases from 0.9 to 1.3 ns toward higher temperatures (Figure 6b,e). The total increase of the absolute values of $A_{fast} + A_{slow}$ at decreasing temperature by a factor of three reflects a strong sensitivity of the optical ground state bleaching to long range ordering of small polarons due to formation of the charge-ordered phase (see also Section 3, Supporting Information).

The stretching factor b_{slow} lies slightly above 1 for low temperatures and shows a strong rise up to a value of 2 between $T = 180$ K and $T = 220$ K. At $T = 220$ K the stretching factor unsteadily falls back to 1, from where it continuously rises up to higher temperatures. This indicates a change in the nature of the underlying process at a temperature range close to the charge-ordering temperature.

2.6. Jahn–Teller Dimer Model

For a detailed analysis of the underlying mechanisms and time scales involved in the hot polaron relaxation, in the following, we introduce a JT dimer model. The model consists of two corner-sharing MnO_6 octahedra sharing one oxygen bridge (**Figure 7**). Each octahedron can undergo two independent JT active distortions and it contains two spin-aligned Mn 3d e_g states forming the polaron. The electrons can hop between the two Mn sites. Here we consider the special case with one electron shared between two Mn sites. The JT dimer with a shared single electron is a minimal model for a Zener polaron,[33–35] which is the dominant feature for the doped (ideally half-doped) manganites. The two Mn ions of the half-doped JT dimer are ferromagnetically aligned, so that the electron delocalizes over both sites, a mechanism that is the so-called double exchange mechanism. Experiments provide structural evidence for Zener polarons.[36,37] They are further supported by the observation, that in the charge-ordered state of PCMO in a doping range of $0.3 \leq x \leq 0.5$, the spatial variation of charge carrier density occurs on oxygen sites,[8] whereas the valence separation between different Mn sites is rather low.[8,38–40]

Since the Mn 3d e_g states have the same parity with respect to the Mn-site, the optical transition between JT split states,

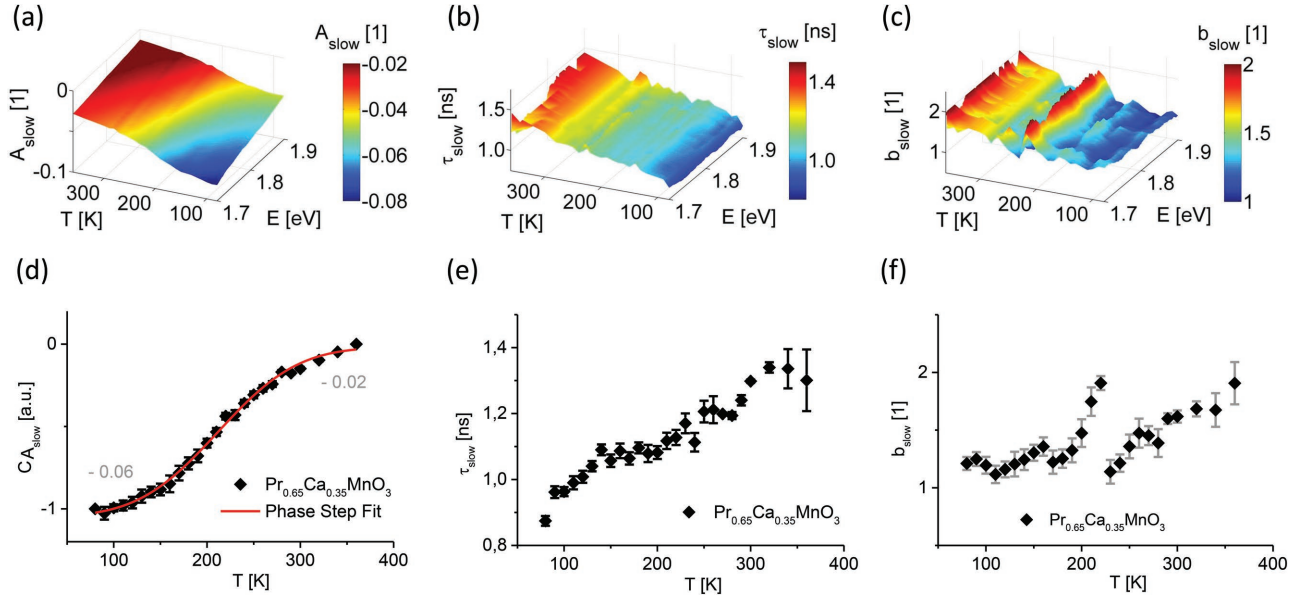

Figure 6. Energy and temperature dependence of the slow relaxation process (iv) in the ΔOD, after photoexcitation at 1.55 eV. a) The amplitude, b) the decay time, and c) the stretching factor of the stretched exponential decay fitting of this process measured at different temperatures between 80 and 360 K. d) Correlation function for the amplitude. A nonlinear phase step fit for the correlation function of the amplitude is illustrated by the red line. The central temperature of the phase transition was fitted to $T = 212(2)$ K with a width of 67(4) K. The medians of the measurements at 80 and 360 K are shown in gray. e) Mean value along the probe energy of the decay time. f) Mean value along the probe energy of the stretching factor.

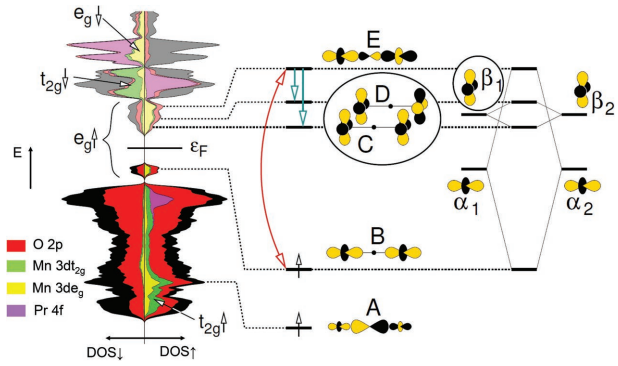

Figure 7. Dipole-allowed polaron transition and subsequent temporal evolution of the hot polaron state, based on the model of a ferromagnetically coupled JT dimer, which forms a Zener polaron. Shown is the schematic orbital diagram of a Zener polaron (right) and its relation to the density of states of $Pr_{0.65}Ca_{0.35}MnO_3$ with CE-type antiferromagnetic order (left) and transitions (middle) as obtained by first-principles calculations. The relevant Mn 3d states are distinguished as e_g states (yellow) pointing toward the oxygen bridges and the t_{2g} orbitals (green). For the magnetic ions Pr and Mn, the density of states is shown only for ions with one spin direction (up).

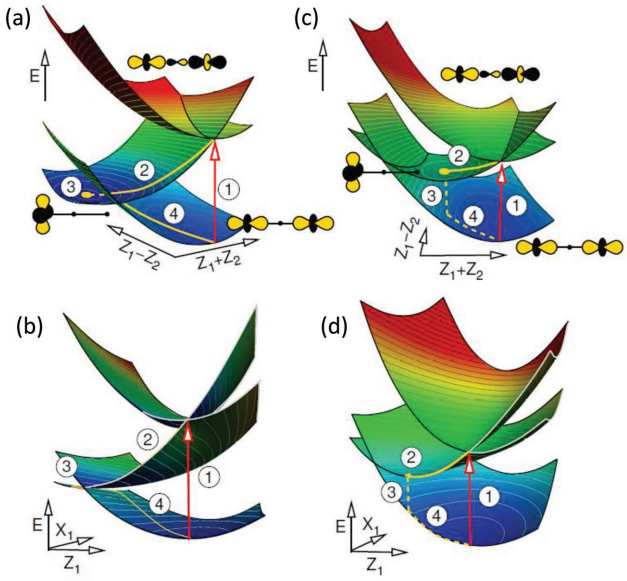

Figure 8. Born–Oppenheimer surfaces relevant for the relaxation process of the JT dimer. On the bottom and top surfaces in each subfigure the electron is in the states with σ-symmetry. On the middle surface the electron has δ-symmetry. The sketches of the states are shown next to the corresponding energy surfaces. The two graphs (a) and (b) consider an isolated JT dimer, while the graphs (c) and (d) account for cooperative effects. a,c) The cut through configuration space with $X_1 = X_2 = 0$, which allows only oblate and prolate distortions of the octahedra along the dimer axis. b,d) The configuration space of one of the octahedra, while the other one is kept at the structure it has in the ground state with $X_2 = 0$ and $Z_2 = 0.5$. An optical excitation (1) takes the electron from the ground state into the antibonding σ-state. From there the electron relaxes onto the middle energy surface (2). Without cooperative effects (left) the system passes through a conical intersection onto the lowest surface (3), from where it can return to the ground state (4) by passing around the conical intersection. By contrast, with sufficiently strong cooperative effects (right), the middle surface exhibits a minimum (2), which can trap the system. It can escape onto the lowest surface either by an optical transition or by a radiation-less thermal process. Recombination (3) of the electron–hole pair is slow because the optical transition is dipole forbidden. The alternative is a thermal fluctuation toward the conical intersection, from where it can pass onto the lowest surface in a radiation-less process.

such as the one from orbital α_1 to β_1 in Figure 7, is dipole forbidden. Symmetry-lowering distortions in the crystal or odd-parity vibrations are unable to explain the observed strong absorption in Figure 1, which reaches 25%–30% of that of the charge-transfer transitions.[12] However, a strong dipole-allowed transition exists in the Zener polaron (Section 13, Supporting Information). Initial and final state of the optical transition, denoted as (B) and (E) in Figure 7, are Mn 3d e_g orbitals of σ-bond character, pointing toward the bridging oxygen ion. These states satisfy the selection rules, because the initial state of the transition (B) is even with respect to a reflection at the mid plane of the dimer, while the final state (E) is odd.

Our ab initio calculations position the final state (E) of the optical transition slightly above the JT partners (C) and (D), i.e., the e_g orbitals with δ-symmetry with respect to the bridging oxygen. They are located slightly below the final state (E) of the optical transition. This indicates that the excited electrons may relax after the optical excitation through a conical intersection into the Mn 3d e_g orbitals, denoted as (C) and (D) in Figure 7. The involved energy surfaces and conical intersections are illustrated in **Figure 8**. We have chosen the parameters of the model so that the conical intersection with the δ-type energy surface is also the minimum of the upper energy surface, this is an idealization. Actually, the energetic separation of the states (E) and the states (C) and (D) indicates, that the highest energy surface has a minimum, which is separated from the conical intersection. Thus, the initial relaxation through the conical intersection, i.e., process (2) in Figure 8, should be thermally activated.

Our model suggests that the population of originally unoccupied JT partners, i.e., states (C) and (D), initiates a structural dynamics. The JT distortions get inverted, which means that the octahedral distortion changes from prolate along the dimer axis to oblate. During this fast structural rearrangement, the excited electron on the δ-type energy surface evolves toward a conical intersection with the ground state energy surface, i.e., the system proceeds to configuration (3). From here the relaxation to ground state via recombination of the electron in states (C) and (D) with the hole in state (B) is symmetry forbidden, i.e., δ- versus σ-bonding. Nevertheless, the system is not trapped in (3) in case of an isolated JT dimer, decoupled from collective behavior of the environment. As shown in Figure 8b, it can pass around the conical intersection with the ground state energy surface and proceed on process (4) toward the ground state.

By contrast, sufficiently strong cooperative effects of the environment shift the position of the minimum on the δ-type potential energy surface. This is modeled by introducing a term accounting for the coupling of the Zener polaron to the environmental bond network (see Section 14, Supporting Information). The resulting minimum of the potential energy surface is then separated from the conical intersection with the ground state energy surface (Figure 8c,d). As mentioned before, radiative

decay, one of the relaxation channels (process (3)), is dipole forbidden and thus slow. The other relaxation channel requires a thermal fluctuation to the conical intersection, through which the system can then escape toward the ground state.

3. Discussion

We rationalize our experimental findings on the basis of the JT dimer model, introduced above. Let us first investigate the optical absorption and the initial fast relaxation step: We argue against the conventional view, that the optical transition is one between the lower and the upper JT split Mn 3d e_g states on a single site (e.g., ref. [18]). Rather do we attribute the absorption band to a transition between two states, labeled (B) and (E) in Figure 7, that are delocalized over two or more sites. The initial relaxation termed process (2) in Figure 8 from state (E) to the states with δ-symmetry (C) and (D) is most likely related to the fast relaxation process (ii) observed in the transient absorbance described by $\tau_{fast} \approx 980$ fs ($\leftrightarrow$ 4.2 meV) at 360 K. The observed slowdown to $\tau_{fast} \approx 1.78$ ps ($\leftrightarrow$ 2.3 meV) at 80 K (Figure 4d) is consistent with the proposed thermally activated process.

The existence of a hot polaron state with a long lifetime in the states (C) and (D) at temperatures below T_{CO} is strongly supported by the observation of a photovoltage at the pump energy $E = 1.55$ eV, which linearly increases with decreasing temperature. Such a behavior proves photoexcited minority carriers with a lifetime long enough for diffusion to the interface of the heterojunction.[41] The limit V_{OC} ($T \rightarrow 0$) gives the barrier of the heterojunction for charge separation It reflects charge separation of the photoexcited minority charge carriers, i.e., electrons, from the majority hole-type carriers in the p-doped PCMO film.[42] A linear fit yields $E_b = 520$ meV, which is close to the value for broadband illumination ($E_b = 547$ meV), showing that the splitting of the chemical potential of electrons and holes under $E = 1.55$ eV illumination is not significantly increased at higher photon energies and thus governed by the energy of the polaronic excitation. Electron beam induced current analysis supports the presence of a finite diffusion length of excited charge carriers in the 10 nm range,[43] consistent with a nanosecond lifetime of the involved excitations at low temperatures. Above T_{CO}, the observed thermally activated behavior of V_{OC} with an activation energy of $E_A = 515 \pm 30$ meV points to an origin from interface-type electron–hole photoexcitation across the interface barrier E_b.

In the following we discuss the process underlying the observed slow ns dynamics of the transient $\Delta OD(t)$, process (iv). Our JT model suggests a strong dependence of the hot polaron lifetime on the dynamics of the octahedral network of the environment. The separation between the hot polaron configuration at the minimum of the energy potential surface of the δ-states from the conical intersection with the ground state energy surface requires a type of cooperative dynamics of the excited MnO_6 octahedra which seems to exist only in the CO state. This generates an energy barrier for hot polaron recombination which determines the lifetime at low temperatures. With a temperature increase to $T > T_{CO}$ the reduced degree of cooperative response in the disordered phase shifts the minimum toward the conical intersection, thus, reducing the barrier height for hot polaron recombination. Accordingly, we would expect a faster decay of the hot polaron state in the disordered phase at $T > T_{CO}$, which is obviously in contradiction to the observed temperature dependence of τ_{slow}, i.e., the increase with increasing temperature from $\tau_{slow} \approx 0.9$ ns at 80 K to $\tau_{slow} \approx 1.3$ ns at room temperature (Figure 6e). The observed τ_{slow} (T) trend is also inconsistent with the conventional Langevin-type recombination mechanism, which considers the collision probability of spatially separated electron-type and hole-type polarons.[44] Since the collision probability is proportional to the excited carrier mobility, which increases with temperature irrespective of the involved phases, the Langevin mechanism would give rise to a reduction of the lifetime with temperature and thus contradicts our experimental finding.

However, as frequently stated in literature, pump pulse induced sample heating and heat diffusion play a role in transient optical spectroscopy of manganites and can give rise to a slow decay of ΔOD (t) in the ns range.[27,45–47] A quantitative evaluation of heating of the PCMO film and heat diffusion into the MgO substrate (Section 16.2, Supporting Information) reveals a heat decay constant and a heat induced optical density change, which are in quite good agreement with τ_{slow} and A_{slow} at room temperature. This and the absence of a photovoltaic effect due to bulk photodiffusion gives strong evidence, that heat diffusion governs the nanosecond process above T_{CO}. By contrast, for $T < T_{CO}$ the heat decay proceeds much faster than the observed slow relaxation, pointing to the predominance of hot polaron lifetime over heat diffusion. In a nutshell, the temperature trend of τ_{slow} can be understood as a transition from hot polaron decay in the CO phase according to process (3) at $T < T_{CO}$ (Figure 8c,d) to a heat diffusion controlled process at $T > T_{CO}$. The strong scattering and discontinuity of the parameter b_{slow} at $T = 220$ K (Figure 6f) supports the change of the relaxation mechanism at the phase transition. The variation range of b_{slow} at $T \approx 220$ K is significantly larger than the error bars, indicating a mechanistic origin of the b_{slow} discontinuity.

A change in the cooperative dynamics at the charge-order transition is furthermore supported by the observed change of the coherent THz dynamics (Figure 5). Our model suggests, that due to the long lifetime of the inverted population of the formerly unoccupied Mn 3d e_g states ((C) and (D)), a cooperative structural dynamics in the THz range (orbital waves) is initiated, being visible as coherent oscillations of the ΔOD. According to Raman spectroscopy by Amelitchev and co-workers the 2 THz coherent oscillation corresponds to an A_g mode, that strongly depends on the A-cation mass and is accordingly attributed to vibrations of Pr/Ca atoms.[48,49] Clearly, introducing disorder into the CO state via long living hot polaron states can induce structural rearrangements, which trigger coherent motion of the Mn, O, and the Pr/Ca atoms. The strong change of the amplitude of the THz oscillations at T_{CO} (Figure 5d) is a consequence of this effect.[50] Other coherent waves include a 25 GHz mode (40 ps oscillation) which can be interpreted as an acoustic strain wave, initiated by a strong lattice expansion in the excited volume at high pump intensities (Section 8, Supporting Information). It propagates back and forth through the entire PCMO film between the films surface and the film-substrate[51] until it disappears due to decoherence and dissipation into heat.

4. Summary and Conclusion

In conclusion, time-resolved transient absorption spectroscopy in combination with photovoltaic measurements provides clear evidence for long-lived polaron-type optical excitations in the strongly correlated manganite PCMO. Of particular interest is the ultraslow relaxation with a decay time of 1–2 ns. At room temperature, conversion of polaronic excitations into heat and diffusion into the substrate is most likely responsible for this slow process. However, based on measurements of the open-circuit voltage of the PCMO/STNO heterojunction, the origin of the long lived state at low temperatures is attributed to a hot polaron, that is a long lived electron–hole polaron pair excitation, which stores energy far from thermal equilibrium. The nature of the hot polaron, its excitation and relaxation processes have been analyzed in detail using a JT dimer as a model for a Zener polaron. Our calculations identify a transition with a large transition matrix element between two states that spread over two Mn sites. Following the excitation, a complex electronic and structural dynamics sets in, which, when isolated, takes the system rapidly back into the ground state via radiation-less transitions through two conical intersections. However, when cooperative effects of the environment are taken into account, the system is trapped in a long-lived hot polaron state.

The implications are quite far reaching, since such long-living states can be the origin for the evolution of optical phase transitions with hidden phases at high photon fluxes.[25] The involved strong dipole allowed transition gives rise to very small optical absorption lengths of less than 150 nm.[42] Consequently, such strongly absorbing hot polarons with long lifetimes may represent an ideal light absorber for harvesting photons in the IR and visible part of the solar spectrum. These results may offer new perspectives for design of nanoscale oxides for hot polaron photovoltaics or photocatalysis.

5. Experimental Section

All presented pump–probe measurements were performed using a homebuilt transient absorption spectrometer with a temporal resolution at the sample position of ≈200 fs. Temperature control of the sample was realized using a commercially available Cryo Cell from Oxford Instruments (Microstat He), where the sample is kept in a moderate vacuum. Further details concerning the setup, analysis of the data as well as the sample preparation can be found within the Supporting Information.

Supporting Information

Supporting Information is available from the Wiley Online Library or from the author.

Acknowledgements

Funding by the Deutsche Forschungsgemeinschaft (DFG) via the CRC 1073, Project B02, B03, C02, and C03, and the CRC 755, Project B03, is gratefully acknowledged. E. Ronge supported the XRD measurements shown in Figure S3 (Supporting Information). S.M. and C.J. prepared the manganite films and performed the structural and the static optical characterization. D.R. and S.T. designed the setup, performed the time-resolved measurements, and analyzed the data. B.I. performed the photovoltaic measurements. M.S. and P.B. performed the computational calculations. All authors contributed to the interpretation of the results and to the writing of the manuscript. The authors declare no competing financial interests.

Received: September 29, 2016
Revised: December 2, 2016
Published online: January 24, 2017

[1] W. A. Tisdale, K. J. Williams, B. A. Timp, D. J. Norris, E. S. Aydil, X.-Y. Zhu, *Science* **2010**, *328*, 1543.
[2] S. Rein, *Lifetime Spectroscopy - A Method of Defect Characterization in Silicon for Photovoltaic Applications*, Vol. *85*, Springer, Berlin **2005**.
[3] D. K. Schroder, *Semiconductor Material and Device Characterization*, 2 ed., John Wiley & Sons, New York **1998**.
[4] K. A. Al-Hassanieh, F. A. Reboredo, A. E. Feiguin, I. González, E. Dagotto, *Phys. Rev. Lett.* **2008**, *100*, 166403.
[5] S. Sayyad, M. Eckstein, *Phys. Rev. B* **2015**, *91*, 104301.
[6] D. Yarkony, Conical Intersections, *Advanced Series in Physical Chemistry*, Vol. *15* (Eds: W. Domcke, D. Yarkony, H. Köppel), World Scientific, Singapore, **2004**, p. 41.
[7] A. Lanzara, N. L. Saini, M. Brunelli, F. Natali, A. Bianconi, P. G. Radaelli, S.-W. Cheong, *Phys. Rev. Lett.* **1998**, *81*, 878.
[8] G. Zhao, Y. S. Wang, D. J. Kang, W. Prellier, M. Rajeswari, H. Keller, T. Venkatesan, C. W. Chu, R. L. Greene, *Phys. Rev. B* **2000**, *62*, R11949.
[9] Ch. Jooss, L. Wu, T. Beetz, R. F. Klie, M. Beleggia, M. A. Schofield, S. Schramm, J. Hoffmann, Y. Zhu, *Proc. Natl. Acad. Sci. USA* **2007**, *104*, 13597.
[10] J. Zhang, R. D. Averitt, *Annu. Rev. Mater. Res.* **2014**, *44*, 19.
[11] Ch. Hartinger, F. Mayr, A. Loidl, T. Kopp, *Phys. Rev. B* **2006**, *73*, 024408.
[12] S. Mildner, J. Hoffmann, Ch. Jooss, P. E. Bloechl, S. Techert, *Phys. Rev. B* **2015**, *92*, 035145.
[13] E. Frankevich, H. Ishii, Y. Hamanaka, T. Yokoyama, A. Fuji, S. Li, K. Yoshino, A. Nakamura, K. Seki, *Phys. Rev. B* **2000**, *62*, 2505.
[14] N. N. Loshkareva, L. V. Nomerovannaya, E. V. Mostovshchikova, A. A. Makhnev, Yu. P. Sukhorukov, N. I. Solin, T. I. Arbuzova, S. V. Naumov, N. V. Kostromitina, A. M. Balbashov, L. N. Rybina, *Phys. Rev. B* **2004**, *70*, 224406.
[15] M. Quijada, J. Černe, J. R. Simpson, H. D. Drew, K. H. Ahn, A. J. Millis, R. Shreekala, R. Ramesh, M. Rajeswari, T. Venkatesan, *Phys. Rev. B* **1998**, *58*, 16093.
[16] J. H. Jung, K. H. Kim, T. W. Noh, E. J. Choi, J. Yu, *Phys. Rev. B* **1998**, *57*, R11043.
[17] Y. Okimoto, Y. Tomioka, Y. Onose, Y. Otsuka, Y. Tokura, *Phys. Rev. B* **1999**, *59*, 7401.
[18] H. A. Jahn, E. Teller, *Proc. R. Soc. London, Ser. A* **1937**, *161*, 220.
[19] E. Dagotto, *Nanoscale Phase Separation and Colossal Magneto-Resistance: The Physics of Manganites and Related Compounds*, Springer Series in Solid-State Sciences, Vol. *136*, Springer, Berlin **2003**.
[20] K. J. Thomas, J. P. Hill, S. Grenier, Y.-J. Kim, P. Abbamonte, L. Venema, A. Rusydi, Y. Tomioka, Y. Tokura, D. F. McMorrow, G. Sawatzky, M. van Veenendaal, *Phys. Rev. Lett.* **2004**, *92*, 237204.
[21] R. Englman, *The Jahn–Teller Effect in Molecules and Crystals*, Wiley, London, **1972**.
[22] R. G. McKinlay, M. J. Paterson, H. Köppel, D. R. Yarkony, H. Barentzen, The Jahn–Teller Effect, *Springer Series in Chemical Physics*, Vol. *97*, Springer-Verlag Berlin Heidelberg, **2009**, p. 311.
[23] K. H. Wu, T. Y. Hsu, H. C. Shih, Y. J. Chen, C. W. Luo, T. M. Uen, J.-Y. Lin, J. Y. Juang, T. Kobayashi, *J. Appl. Phys.* **2009**, *105*, 043901.

[24] Y. H. Ren, M. Ebrahim, Z. A. Xu, G. Lüpke, *New J. Phys.* **2009**, *11*, 113013.
[25] H. Ichikawa, S. Nozawa, T. Sato, A. Tomita, K. Ichiyanagi, M. Chollet, L. Guerin, N. Dean, A. Cavalleri, S. Adachi, T. Arima, H. Sawa, Y. Ogimoto, M. Nakamura, R. Tamaki, K. Miyano, S. Koshihara, *Nat. Mater.* **2011**, *10*, 101.
[26] Y. H. Ren, M. Ebrahim, H. B. Zhao, G. Lüpke, Z. A. Xu, V. Adyam, Q. Li, *Phys. Rev. B* **2008**, *78*, 014408.
[27] J. Bielecki, R. Rauer, E. Zanghellini, R. Gunnarsson, K. Dörr, L. Börjesson, *Phys. Rev. B* **2010**, *81*, 064434.
[28] W. Shockley, *Bell Syst. Tech. J.* **1949**, *28*, 435.
[29] S. M. Sze, *Physics of Semiconductor Devices*, Wiley-Interscience, New York, USA **1969**.
[30] S. Y. Zhou, M. C. Langner, Y. Zhu, Y.-D. Chuang, M. Rini, T. E. Glover, M. P. Hertlein, A. G. Cruz Gonzalez, N. Tahir, Y. Tomioka, Y. Tokura, Z. Hussain, R. W. Schoenlein, *Sci. Rep.* **2014**, *4*, 4050.
[31] P. Beaud, A. Caviezel, S. O. Mariager, L. Rettig, G. Ingold, C. Dornes, S.-W. Huang, J. A. Johnson, M. Radovic, T. Huber, T. Kubacka, A. Ferrer, H. T. Lemke, M. Chollet, D. Zhu, J. M. Glownia, M. Sikorski, A. Robert, H. Wadati, M. Nakamura, M. Kawasaki, Y. Tokura, S. L. Johnson, U. Staub, *Nat. Mater.* **2014**, *13*, 923.
[32] J. Hoffmann, P. Moschkau, S. Mildner, J. Norpoth, Ch. Jooss, L. Wu, Y. Zhu, *Mater. Res. Express* **2014**, *1*, 046403.
[33] G. Zheng, C. H. Patterson, *Phys. Rev. B* **2003**, *67*, 220404.
[34] C. de Graaf, C. Sousa, R. Broer, *Phys. Rev. B* **2004**, *70*, 235104.
[35] C. H. Patterson, *Phys. Rev. B* **2005**, *72*, 085125.
[36] A. Daoud-Aladine, J. Rodríguez-Carvajal, L. Pinsard-Gaudart, M. T. Fernández-Díaz, A. Revcolevschi, *Phys. Rev. Lett.* **2002**, *89*, 097205.
[37] L. Wu, R. F. Klie, Y. Zhu, Ch. Jooss, *Phys. Rev. B* **2007**, *76*, 174210 .
[38] S. Grenier, J. P. Hill, D. Gibbs, K. J. Thomas, M. v. Zimmermann, C. S. Nelson, V. Kiryukhin, Y. Tokura, Y. Tomioka, D. Casa, T. Gog, C. Venkataraman, *Phys. Rev. B* **2004**, *69*, 134419.
[39] J. García, M. C. Sánchez, G. Subías, J. Blasco, *J. Phys.: Condens. Matter* **2001**, *13*, 3229.
[40] D. Mierwaldt, S. Mildner, R. Arrigo, A. Knop-Gericke, E. Franke, A. Blumenstein, J. Hoffmann, Ch. Jooss, *Catalysts* **2014**, *4*, 129.
[41] S. S. Perlman, D. L. Feucht, *Solid-State Electron.* **1964**, *7*, 911.
[42] G. Saucke, J. Norpoth, Ch. Jooss, D. Su, Y. Zhu, *Phys. Rev. B* **2012**, *85*, 165315.
[43] B. Ifland, P. Peretzki, B. Kressdorf, P. Saring, A. Kelling, M. Seibt, Ch. Jooss, *Beilstein J. Nanotechnol.* **2015**, *6*, 1467.
[44] U. Albrecht, H. Baessler, *Phys. Status Solidi B* **1995**, *191*, 455.
[45] Y. M. Sheu, S. A. Trugman, L. Yan, J. Qi, Q. X. Jia, A. J. Taylor, R. P. Prasankumar, *Phys. Rev. X* **2014**, *4*, 021001.
[46] H. Tamaru, K. Ishida, N. Ogawa, Y. Kubo, K. Miyano, *Phys. Rev. B* **2008**, *78*, 075119.
[47] T. Ogasawara, T. Kimura, T. Ishikawa, M. Kuwata-Gonokami, Y. Tokura, *Phys. Rev. B* **2001**, *63*, 113105.
[48] V. A. Amelitchev, B. Güttler, O. Y. Gorbenko, A. R. Kaul, A. A. Bosak, A. Y. Ganin, *Phys. Rev. B* **2001**, *63*, 104430.
[49] P. Beaud, S. L. Johnson, E. Vorobeva, U. Staub, R. A. De Souza, C. J. Milne, Q. X. Jia, G. Ingold, *Phys. Rev. Lett.* **2009**, *103*, 155702.
[50] D. Lim, V. K. Thorsmølle, R. D. Averitt, Q. X. Jia, K. H. Ahn, M. J. Graf, S. A. Trugman, A. J. Taylor, *Phys. Rev. B* **2005**, *71*, 134403.
[51] T. Ogasawara, M. Matsubara, Y. Tomioka, M. Kuwata-Gonokami, H. Okamoto, Y. Tokura, *Phys. Rev. B* **2003**, *68*, 180407(R).